ARMY RESEARCH LABORATORY

Examination of the Thermal Ignition of M30 Propellant by Residual Steel Fragments

by Kyle Bates, Martin Raftenberg, Hubert Meyer, and Norman Gerri

ARL-TR-4242 **September 2007**

NOTICES

Disclaimers

The findings in this report are not to be construed as an official Department of the Army position unless so designated by other authorized documents.

Citation of manufacturer's or trade names does not constitute an official endorsement or approval of the use thereof.

Destroy this report when it is no longer needed. Do not return it to the originator.

Army Research Laboratory

Aberdeen Proving Ground, MD 21005-5068

ARL-TR-4242 **September 2007**

Examination of the Thermal Ignition of M30 Propellant by Residual Steel Fragments

Kyle Bates, Martin Raftenberg,
Hubert Meyer, and Norman Gerri
U.S. Army Research Laboratory
Survivability and Lethality Analysis Directorate
Weapons and Materials Research Directorate

REPORT DOCUMENTATION PAGE

Form Approved
OMB No. 0704-0188

1. REPORT DATE *(DD-MM-YYYY)*	2. REPORT TYPE	3. DATES COVERED (From - To)
September 2007	Final	

4. TITLE AND SUBTITLE
Examination of the Thermal Ignition of M30 Propellant by Residual Steel Fragments

5a. CONTRACT NUMBER

5b. GRANT NUMBER

5c. PROGRAM ELEMENT NUMBER

6. AUTHOR(S)
Kyle Bates, Martin Raftenberg, Hubert Meyer, and Norman Gerri

5d. PROJECT NUMBER

5e. TASK NUMBER

5f. WORK UNIT NUMBER

7. PERFORMING ORGANIZATION NAME(S) AND ADDRESS(ES)
U.S. Army Research Laboratory
Survivability/Lethality Analysis Directorate
ATTN: AMSRD-ARL-SL-BE
Aberdeen Proving Ground, MD 21005-5068

8. PERFORMING ORGANIZATION REPORT NUMBER
ARL-TR-4242

9. SPONSORING/MONITORING AGENCY NAME(S) AND ADDRESS(ES)
U.S. Army Research Laboratory
2800 Powder Mill Road
Adelphi, MD 20783-1197

10. SPONSOR/MONITOR'S ACRONYM(S)

11. SPONSOR/MONITOR'S REPORT NUMBER(S)
ARL-TR-4242

12. DISTRIBUTION/AVAILABILITY STATEMENT
Approved for public release; distribution is unlimited.

13. SUPPLEMENTARY NOTES

14. ABSTRACT
We report the results of a set of experiments designed to determine the threshold ignition striking velocity (V_s) of fragment simulating projectiles (FSP) that perforate a plate of titanium armor and come to rest in a bed of M30 propellant. A subset of experiments, which focus on an 830 grain (gr) FSP shot through 0.25 in. thick titanium, are modeled using physics-based computer codes. The modeling approach employs two codes in series, an Eulerian shock-physics code (CTH) to model the armor perforation event and a Lagrangian hydrocode (LS-DYNA) to model the thermal conduction between the FSP and propellant. The computer modeling was designed in the interest of creating predictive methodology for evaluating survivability and lethality. The research was funded by the U.S. Army Research Laboratory (ARL) Director's Research Initiative.

15. SUBJECT TERMS
thermal ignition, M30, CTH, LS-DYNA, FSP, heat conduction, ammunition vulnerability, propellant vulnerability

16. SECURITY CLASSIFICATION OF:			17. LIMITATION OF ABSTRACT	18. NUMBER OF PAGES	19a. NAME OF RESPONSIBLE PERSON
a. REPORT	b. ABSTRACT	c. THIS PAGE			Kyle Bates
U	U	U	SAR	30	19b. TELEPHONE NUMBER (*Include area code*) (410) 278-3052

Standard Form 298 (Rev. 8/98)
Prescribed by ANSI Std. Z39.18

Contents

List of Figures

List of Tables

Preface

The objective of this research was to develop a primarily physics-based methodology capable of predicting the conductive thermal ignition of energetic materials by residual fragments. The intended application of this methodology is to provide input for survivability and lethality analyses. Our research used a combination of ballistic range experimentation and computer simulations to develop the methodology described in this report.

Acknowledgment

The authors thank Fred Marsh, Paul “Danny” Dominick, and their staff of the U.S. Army Research Laboratory (ARL), Survivability/Lethality Analysis Directorate (SLAD) for their help and the generous use of the ARL/SLAD’s Experimental Facility 6 (EF6) during the ignition threshold velocity experiments.

1. Introduction

With the current emphasis on faster, lightly-armored vehicles, small and medium caliber-sized threats are a greater concern than they would be with traditional, heavily-armored vehicles. Aside from the mechanical damage expected from perforating threats, there is an added concern about the vulnerability of energetic materials such as propellants, explosives, and fuel (*1*). The ignition of energetic materials by a single projectile has the potential to cause a greater amount of large-scale damage than a single projectile is capable of alone.

The threat of thermal ignition by fragments occurs from the heating induced when a fragment perforates armor and is plastically deformed. As a fragment penetrates an armor plate, it is locally heated to high temperatures in the regions where the majority of plastic work has occurred. When these heated residual fragments come into contact with the energetic material behind the armor, they can conduct enough heat to trigger the material to ignite (*2*) and, subsequently, cause significant damage to personnel and vehicles. Energetic materials can also be ignited by fragments through shock compression, if the residual fragments have high velocities. However, this research pertains to relatively low residual velocities (V_r) and focuses on the conductive thermal ignition regime.

Energetic materials react in a number of ways to ignition, which are (in ascending order of reaction speed and violence): burn, fast burn, deflagration, explosion, partial detonation, and detonation (*3*). The energetic material addressed in this research was M30A1 tank gun propellant. In our experiments, we only observed reactions in the burn to fast burn regimes.

2. Approach

Our research focused on a simplified threat-target pair that is representative of medium caliber penetrators or high explosive (HE) munitions fragments and light-armor. The penetrators we studied were 4340 steel, right circular cylinder (RCC) fragment simulating projectiles (FSPs) with masses of 208 and 830 grains (gr), or 0.5 caliber (cal) and 20 mm, respectively. The FSP masses are representative of fragments generated by large HE fragmenting munitions. The target material was titanium, precisely; Ti-6Al-4V extra-low interstitial (ELI) annealed plates with thicknesses of 0.25 and 0.5 in.

2.1 Ballistic Experiment Approach

Two types of ballistic experiments were carried out to support this research: ignition threshold velocity shots and V_r shots. We conducted each of the two types of experiments for two combinations of FSP mass and titanium plate thickness, 830 gr FSP vs. 0.25 in. thick titanium and 208 gr FSP vs. 0.25 in. thick titanium.

2.1.1 Ignition Threshold Velocity Experiments

The first set of experiments was designed to measure the ignition threshold velocity for a given FSP. The ignition threshold velocity is the FSP striking velocity (V_s). We observed nearly all the higher velocities will cause ignition, while the lower velocities will not. We shot the FSPs at 0° obliquity through the titanium plates. The titanium plates covered the only open side of wooden boxes containing M30A1 gun propellant. The boxes were lined with fire-resistant gypsum board and had internal dimensions of 18×12×12 in. A 0.5 in. thick square of Nomex felt was placed directly behind the titanium plate to slow the residual FSP without further deforming it. Slowing the FSP after perforation helped ensure minimal, if any, heating was done in the propellant by shock deformation. The M30A1 propellant grains were loosely packed in the box behind the titanium plate and Nomex felt. Pieces of Celotex and high density foam, usually totaling 6 in. thick, were used to fill the remaining volume in the back of the boxes. The FSP V_s were measured with radar, and a video camera recorded each impact and subsequent propellant reaction, if one occurred. Figure 1 shows a schematic of the ignition shot experimental setup and figures 2a and 2b show images of the setup.

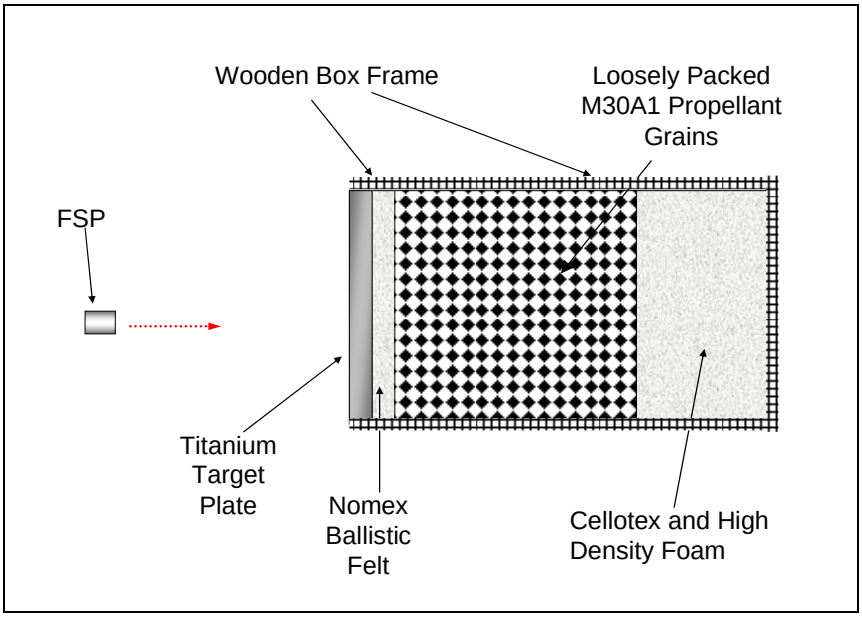

Figure 1. A schematic of the ignition shot experimental setup.

Figure 2a. An image of a box with its top removed.

Figure 2b. An image of a box ready to be shot.

NOTE: The FSP is shot through the hole in the grey steel brace on the front of the box. The brace is used to keep the box in place in the event of a propellant reaction.

2.1.2 Residual Velocity Experiments

Once the ignition threshold impact velocities were determined, the resulting V_r of the fragments needed to be established. For the V_r experiments, we shot the FSPs through the titanium plates and measured the V_r using flash X-ray radiographs. Each fragment-plate combination was shot at its observed ignition threshold velocity. The plates were free-standing without the boxes from the ignition shots. These V_r data were used to assist in validating an Eulerian shock-physics code (CTH) computer model discussed in the next section.

2.2 Computer Simulation Approach

Due to time restraints, the computer simulations focused on the 830 gr FSP vs. 0.25 in. thick titanium combination. This combination was chosen because it provided the most consistent results and presented an apparently distinct ignition threshold V_s.

In order to accurately model the entire armor perforation and thermal ignition event, we used two computer codes, CTH and a Lagrangian hydrocode (LS-DYNA). We chose CTH to model the armor perforation event. The CTH requires the use of the Courant stability criterion (CSC), which requires small time steps in CTH ($\sim 10^{-8}$ s for the armor perforation simulation). The small time steps make heat conduction calculations using CTH unreasonable over the +2 s required to perform the entire simulation. The LS-DYNA allows for suppression of the CSC, and subsequently, allows for longer time steps. We chose to use LS-DYNA to run the heat conduction calculations, because the CSC is irrelevant to heat conduction. The output, from LS-DYNA, allowed us to predict ignition of the propellant.

The process of coupling the data between CTH and LS-DYNA was a non-trivial step. The fundamental differences in the two codes made it difficult to translate the data between them. However, a simple coupling solution was developed by Raftenberg and Meyer, and is described in detail in references 4 and 5.

Measurements from both experimental sets were used to feed the CTH model inputs. The three-dimensional (3D) CTH penetration simulation modeled the impact of the steel FSP against the titanium plate at the ignition threshold V_s. The main CTH outputs were the residual geometry of the steel FSP and its 3D temperature profile. The CTH calculated the temperature increment of each cell in the mesh by dividing the work increment by the specific heat in each time step. The heat conduction was neglected in these CTH calculations because it was irrelevant over the 200 μs long event. Figure 3 shows the steel and titanium regions of the CTH simulation at 200 μs after impact.

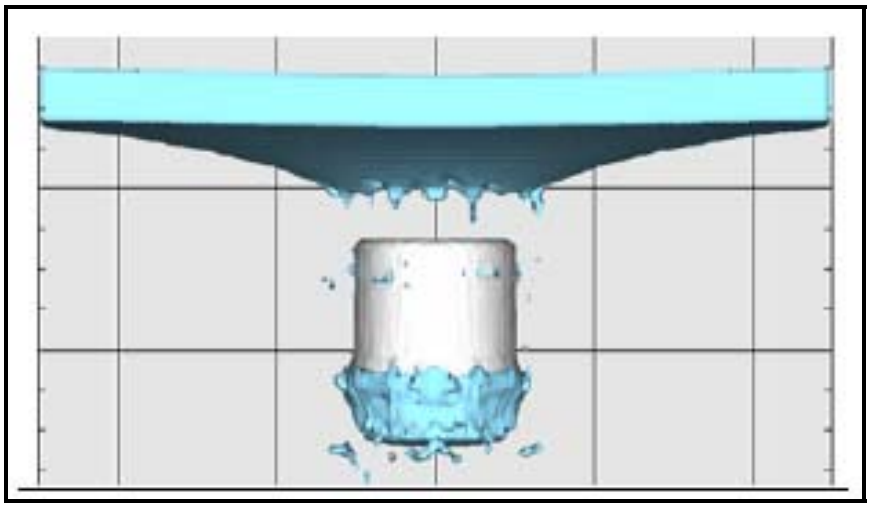

Figure 3. CTH output for the 830 gr steel FSP vs. 0.25 in. titanium plate at 200 μs after impact. The steel material is colored grey, while the titanium material is blue (*4*).

In a late review of the data, we discovered the density and dilation constants for the equation of state input into the CTH model were for aluminum instead of titanium. All of the other model inputs, including those for strength and fracture, were correct. However, because aluminum is less dense than titanium, it is safe to assume that the target material represented in our CTH model provided slightly less ballistic resistance to the FSP projectile than would titanium with accurate equation of state inputs. A detailed description of the inputs used is provided in reference 4 and 5.

The CTH output data were read in an intermediate processing step using EnSight and HyperMesh, a visualization and meshing software, respectively. This combination of software translated the 3D geometry and temperature profile data into a format acceptable by LS-DYNA. Again, reference 4 and 5 discuss this intermediate step between CTH and LS-DYNA at length.. The LS-DYNA simulation modeled a single M30A1 propellant grain in intimate contact with the leading edge of the FSP. The leading edge is the hottest region of the residual FSP, because it is the region that experiences the highest plastic strain. However, because our analysis used a simplified geometry, the propellant was not in contact with the nodes of the residual FSP that CTH determined to be the absolute hottest. The initial conditions for the LS-DYNA simulation are reproduced in figures 4a–4c.

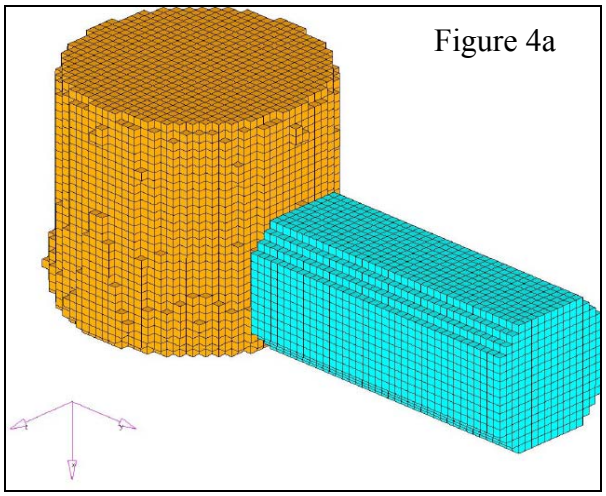

Figure 4a. The steel material is colored orange, while the M30A1 propellant grain is colored blue.

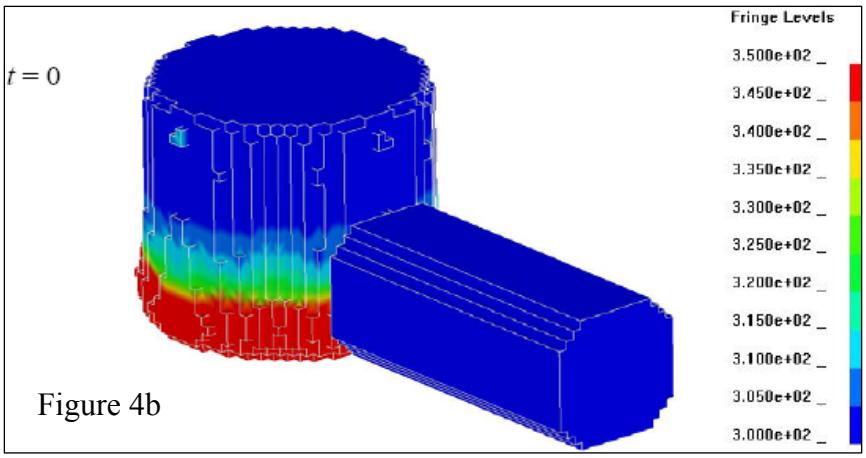

Figure 4b. Surface temperature contours of the LS-DYNA initial conditions. The propellant grain is room temperature and the FSP is heated around the plastically deformed leading edge.

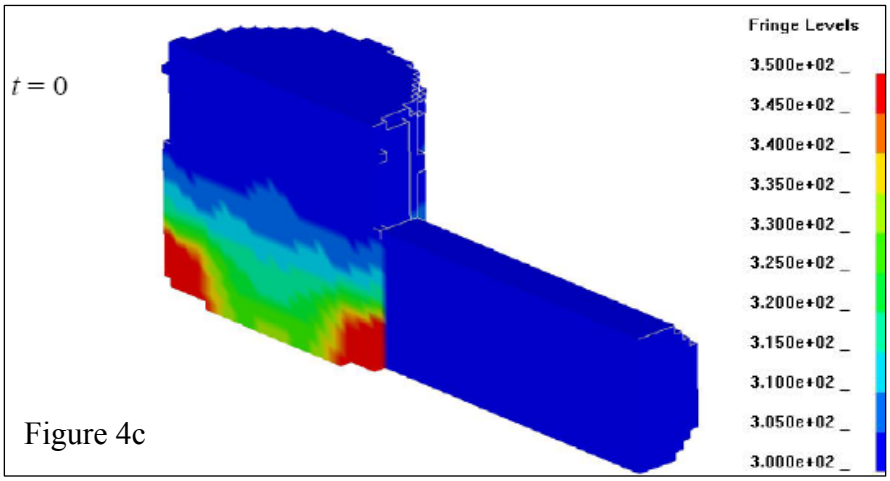

Figure 4c. Initial temperature contours in the mid-plane of the LS-DYNA simulation.

The LS-DYNA heat conduction simulation calculated the 3D thermal conduction between the FSP and propellant grain. Deformation and motion were neglected in the LS-DYNA model because we assumed that the residual FSP comes to rest before any heating occurs in the propellant. The heat from the hottest region of the FSP flowed into the propellant grain and into the cooler regions of the FSP.

3. Results

3.1 Experimental Ballistics Results

The data presented below in Table 1 display the results of the ignition threshold velocity shots for the 208 gr FSP vs. 0.5 in. titanium plate combination.

Table 1. Results from the ignition threshold velocity experiments for the 208 gr FSP.

Shot No.	FSP Mass (gr)	Ti64 Target Thickness (in.)	V_s (m/s)	Burn?
1	208	0.50	807	No
2	208	0.50	810	No
3	208	0.50	819	No
4	208	0.50	836	No
5	208	0.50	839	No
6	**208**	**0.50**	**847**	**Yes**
7	**208**	**0.50**	**848**	**Yes**
8	**208**	**0.50**	**856**	**Yes**
9	208	0.50	869	No
10	208	0.50	871	No
11	**208**	**0.50**	**878**	**Yes**
12	**208**	**0.50**	**892**	**Yes**
13	**208**	**0.50**	**913**	**Yes**

In shot numbers 1, 2, 3, 4, 7, and 9, we observed a phenomenon where the residual steel FSP was encased by a titanium plug or pieces of titanium spall. The titanium covered the FSPs with varying degrees of completeness. In shot numbers 1, 2, and 3 the entire residual FSPs, excluding the rear faces, were covered by titanium. In these cases, the hot leading edges of the FSPs were completely obstructed from direct contact with the propellant by titanium. Figure 5a shows the residual FSP and titanium plug from shot number 2, which is representative of shot numbers 1 and 3 as well. In shot numbers 4, 7, and 9, a titanium spall ring covered only a portion of the FSP, leaving the front face, rear face, and some of the hot leading edge exposed. Figure 5b shows shot number 7, and indicates where the heated leading edge would be exposed to direct contact with propellant.

Figure 5a. Residual FSP from shot number 2.

NOTE: The leading edge of the FSP is completely covered by the titanium plug. This residual formation is also representative of shot numbers 1 and 3.

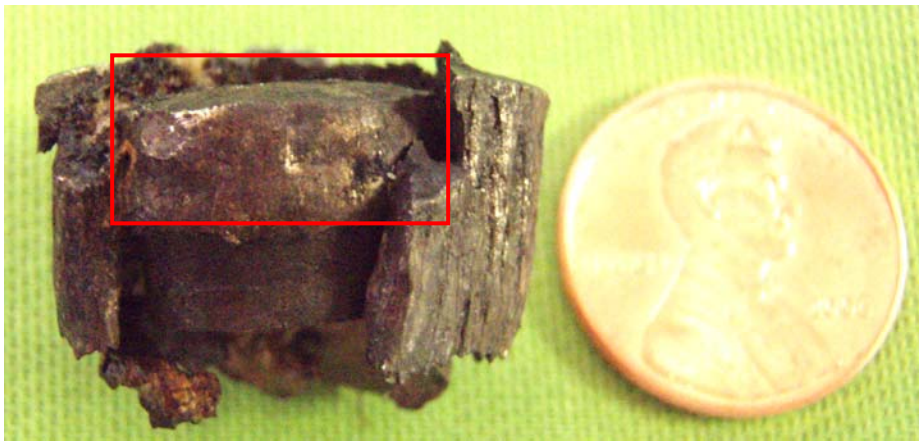

Figure 5b. Residual FSP from shot number 7.

NOTE: The Ti plug and steel FSP are charred black because this residual was involved in a propellant burn reaction. The red box highlights the exposed section of the FSP's plastically deformed leading edge. The Ti spall ring completely covers the rest of the leading edge. This residual formation is also representative of shot numbers 4 and 9.

Based on these qualitative observations and the ignition threshold velocity data in table 1, we did not settle on a single approximate ignition threshold velocity. However, the data seem to suggest that it lies between 840 and 880 m/s.

Figure 6 shows the results from the V_r shots. Because we did not set a distinct ignition threshold velocity for this FSP-target thickness combination, we did not extrapolate a corresponding distinct V_r.

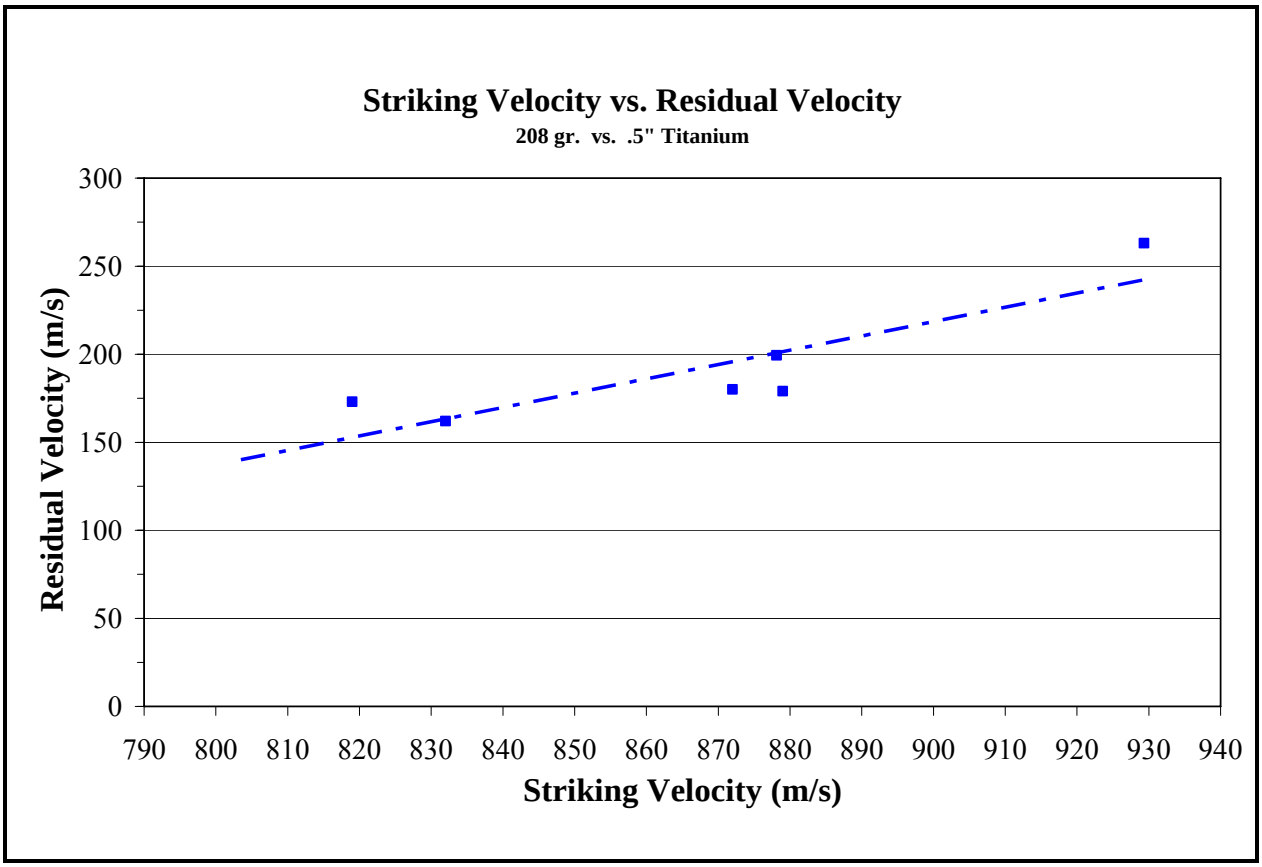

Figure 6. A graph of data from the V_r experiments displays V_s vs. the corresponding V_r.

The inconsistencies and strange plugging phenomenon observed in the 208 gr FSP set of experiments contributed to our decision to focus on modeling the 830 gr FSP set of experiments in the computer simulation.

The data presented below in table 2 display the results of the ignition threshold velocity shots for the 830 gr FSP vs. 0.25 in. titanium plate combination.

Table 2. Results from the ignition threshold velocity experiments for the 830 gr FSP.

Shot Number	FSP Mass (gr)	Ti64 Target Thickness (in.)	V_s (m/s)	Burn?
1	830	0.25	413	No
2	830	0.25	424	No
3	830	0.25	429	No
4	830	0.25	429	No
5	**830**	**0.25**	**431**	**Yes**
6	**830**	**0.25**	**432**	**Yes**
7	830	0.25	433	No
8	830	0.25	434	No
9	**830**	**0.25**	**464**	**Yes**
10	**830**	**0.25**	**482**	**Yes**
11	**830**	**0.25**	**512**	**Yes**

The perforating 830 gr FSPs also induced plugging in the 0.25 in. thick titanium, but the plugs were not large enough to cover the FSP, and they were always clearly separated from the residual steel fragments.

In shot number 3, smoke was observed emitting from the box for +15 s before it eventually stopped and was deemed a "No Burn." Shot 5 was also notable, in that it took a longer time than most shots to initiate a burn, ~8 s after impact, compared to an ignition time of <3 s for most other shots. Based on these observations and the data in the table 2, we settled on an ignition threshold velocity of 433 m/s for the 830 gr vs. 0.25 in. titanium plate.

Figure 7 shows the results from the V_r shots. These data were used to extrapolate an experimental V_r for our ignition threshold V_s of 433 m/s. The solid green line indicates where ignition threshold velocity of 433 m/s intersects the linear fit to give an expected V_r of ~205 m/s. This data was used to help confirm the validity of the CTH model.

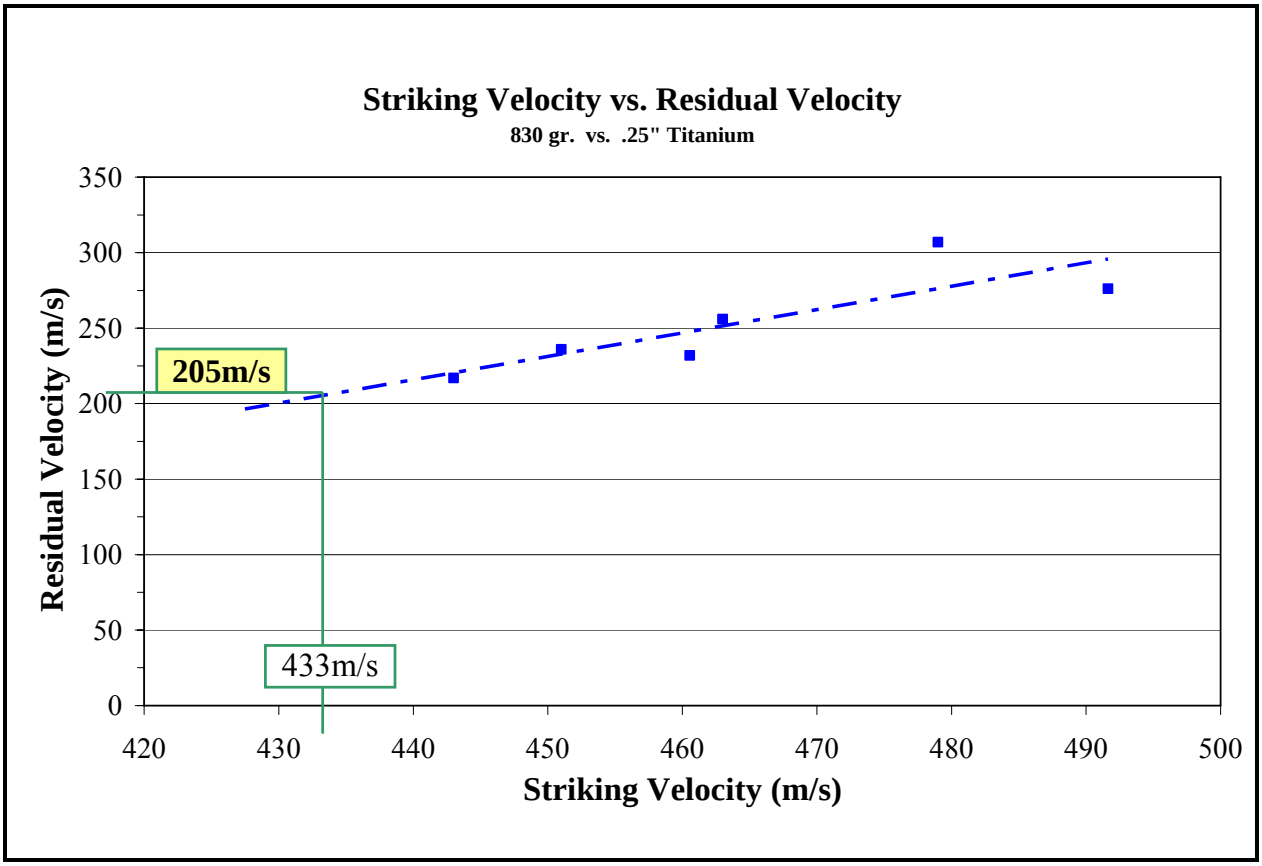

Figure 7. A graph of data from the V_r experiments displays V_s vs. the corresponding V_r. For the ignition threshold V_s of 433 m/s, a V_r of 205 m/s is extrapolated from the linear fit line.

3.2 Computer Simulations Results

3.2.1 CTH

The results reported in this section apply only to the 830 gr FSP vs. 0.25 in. thick titanium plate combination.

The CTH calculated a V_r of 215 m/s. This was very close to the experimental V_r results, 205 m/s, reported in figure 7. Figure 8 shows the X dimension velocity of the FSP as calculated by the CTH. The X dimension is positive down range; normal from the target. The V_r is taken as the velocity of the FSP at 200 μs when it completely exits the titanium plate.

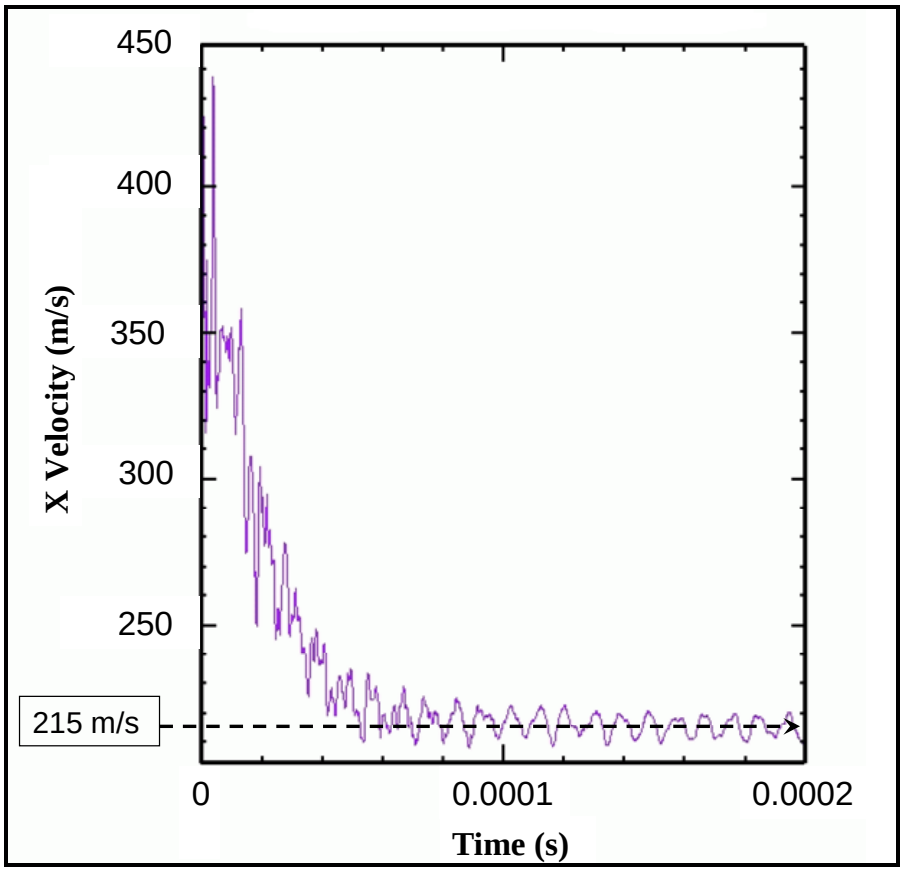

Figure 8. V_r of the 830 gr FSP in CTH is measured at 200 μs, when the FSP exits the titanium plate.

NOTE: The oscillations observed in the velocity graph are due to shock waves reverberating in the FSP.

The residual geometry, of the FSP produced by the CTH, showed deformation in the FSP's leading edge that was consistent with the deformation geometry observed in the live experiments. A sample comparison between a real FSP and the CTH geometry is shown in Figure 9a and 9b.

Figure 9a. Photo of a real initial FSP (left) and real residual FSP (right).

NOTE: The residual in this photo was recovered from the ignition threshold velocity Shot Number 7. It had a striking velocity equal to the ignition threshold velocity of 433 m/s. The scale in the photo is in cm.

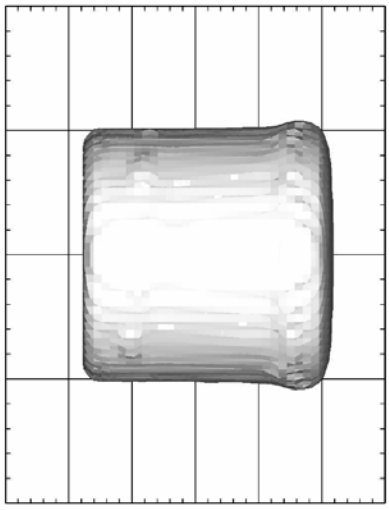

Figure 9b. An image of the residual FSP geometry produced from the CTH results.

NOTE: The scale of the image frame is 4 cm vertically by 3 cm horizontally. The small stabilizing fin on the rear of the real FSPs was not included in the CTH model.

The average measured bulge diameter of the residual FSPs shot at or near the ignition threshold velocity of 433 m/s was ~2.25 cm, a 12.5% increase. The bulge diameter of the residual FSP generated by CTH was 2.17 cm, an 8.5% increase. The initial FSP diameter, for both the real and simulated, was 2.00 cm.

Figure 10 shows the temperature fields calculated by CTH for a residual FSP with V_s of 433 m/s.

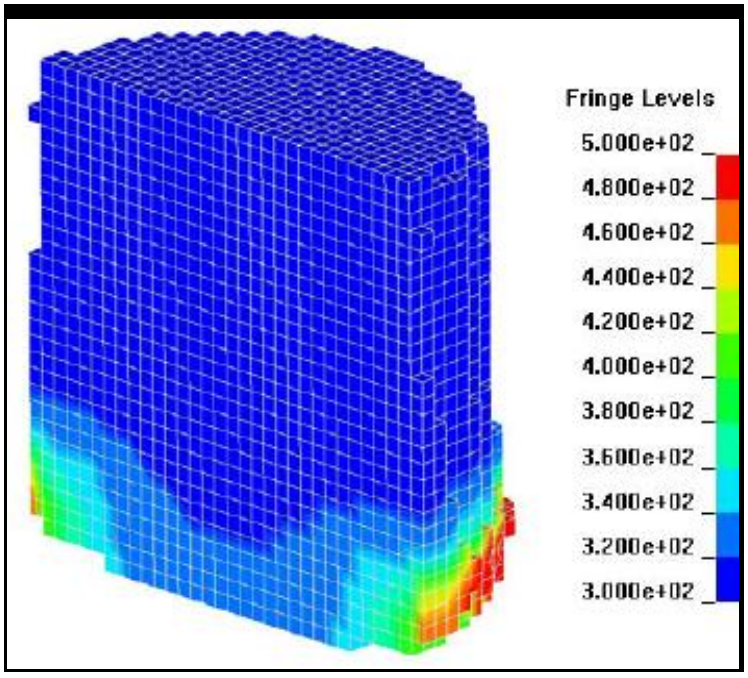

Figure 10. Temperatures within the midplane of the residual FSP as calculated by CTH at t = 200 μs (*4*).

NOTE: The hottest region is the leading edge of the RCC, which underwent the most plastic deformation, while the rest of the FSP is relatively cool. These results are applied as initial conditions in the LS-DYNA analysis. (The fringe levels are kelvin.)

3.2.2 LS-DYNA

The CTH results shown in figure 10 are the initial conditions for the residual FSP in LS-DYNA which are also shown in figure 4 along with the adjacent propellant grain.

Figure 11 shows the initial temperature field on the face of the propellant grain in direct contact with the steel residual, face *A* (*x, z* plane). Face *B* is the plane of propellant material recessed one element dimension, 0.635 mm, into the grain and along the *y* axis, from face *A*. Nodes 1A through 6A are the six hottest nodes in face *A* and are shared by the steel residual. Nodes 1B through 6B are their counterparts with the same *x* and *z* coordinates but on face *B*.

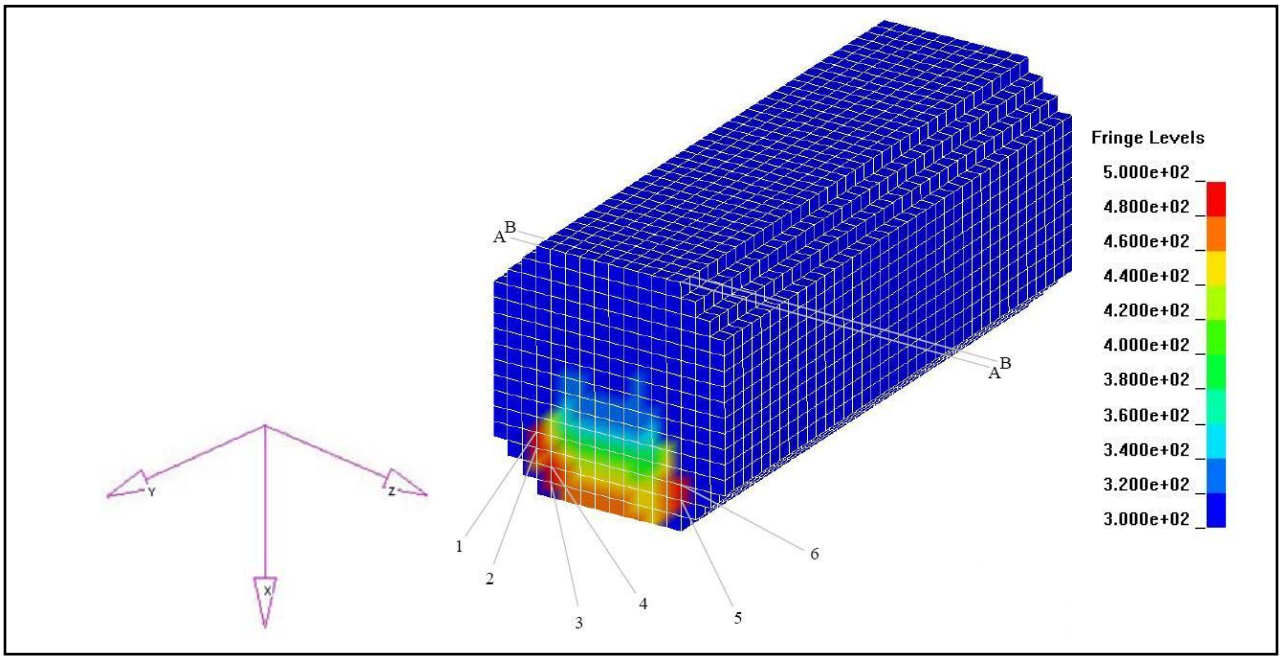

Figure 11. The initial temperature field in the M30A1 grain and the six-nodes and two-faces (A and B) for which temperature histories are recorded in figure 12 (*4*).

Heat from the highly deformed region of the FSP flows faster into the unheated regions of the FSP than into the adjacent propellant grain. This is due to the higher thermal conductance in the steel, 38.11 W/m·K (*6*), compared to a 0.418 W/m·K (*7*) conductance in the M30A1. This effect can be observed in figure 12. Ignition occurs if enough heat is drawn into the propellant grain to reach an ignition threshold temperature before the unheated region of the FSP conducts it away.

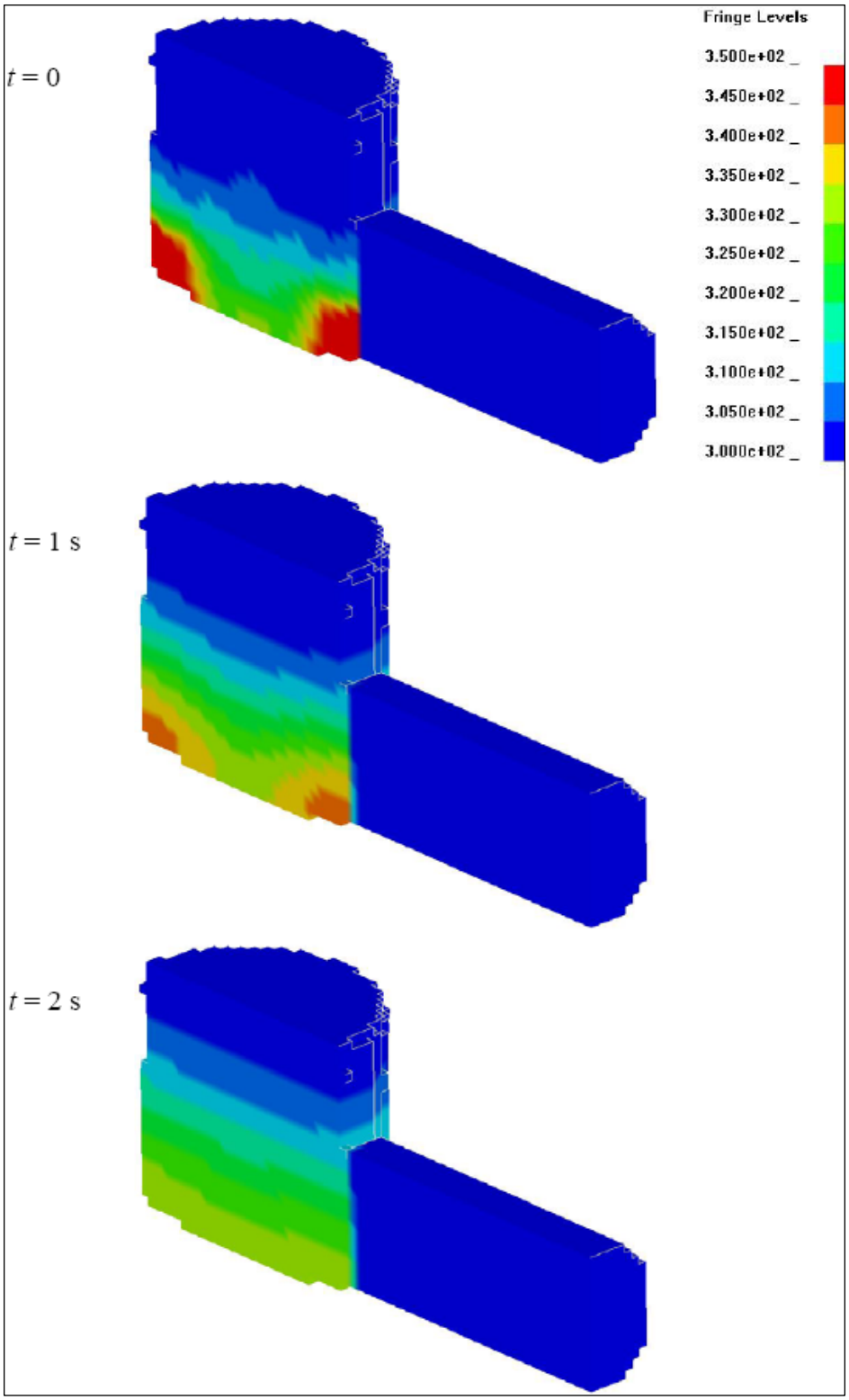

Figure 12. Temperature contours in the midplane of residual FSP and propellant grain at 1 and 2 s after initial contact (*4*). The fringe levels are kelvin.

Figure 13 shows a representative temperature history of the hottest regions in the M30A1 propellant. The location of nodes 6A and 6B are defined in figure 11. Node 6A begins at 524 K. At 2.4 s, temperatures of nodes 6A and 6B have converged to 328 K and 308 K, respectively, suggesting that no further heating occurs in the propellant after 2.4 s.

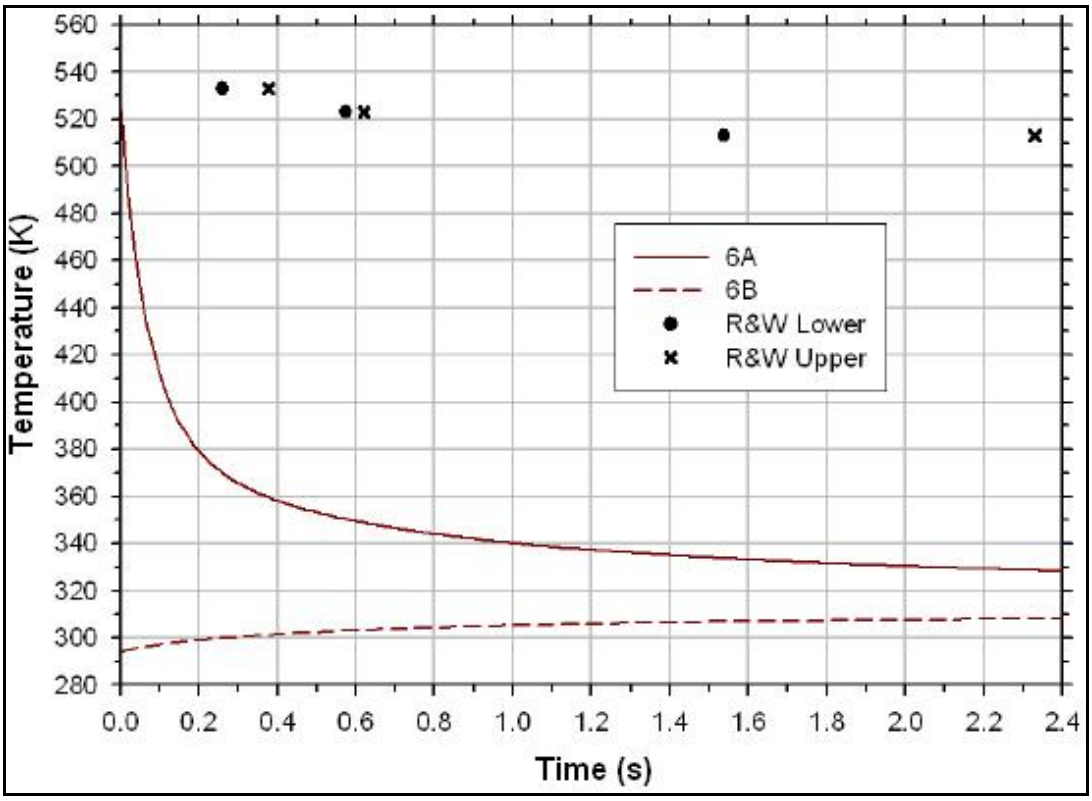

Figure 13. Temperature (K) vs. time (s) at two representative nodes identified in figure 11, one on face A and one on face B (*4*), and ignition times reported in Rocchio and Wires (*2*).

The data points in figure 13 labeled "R&W Lower" and "R&W Upper" refer to M30 ignition data reported by Rocchio and Wires (R&W) (*2*). Rocchio and Wires performed temperature controlled experiments on single grains of M30. For a range of temperatures between 483 K and 533 K, the time required for ignition was measured. Their results, after converting from Celsius to kelvin, are reproduced in table 3. In our experiments, most ignitions occurred 2–3 s after perforation of the titanium. However, some ignitions occurred at upwards of 8 s.

Table 3. Results from the R&W temperature controlled ignition experiments for single grains of M30 propellant grains.

Temperature (K)	t_{lower} (s)	t_{upper} (s)
533	0.260	0.378
523	0.574	0.621
513	1.538	2.329
503	3.422	4.111
493	6.257	7.045
483	9.400	18.256

To quote from R&W, "the high limit was that time above which one could always expect sustained combustion and the low limit was that time below which sustained combustion did not occur" (p. 14). These data are the basis for an initiation criterion to apply to the LS-DYNA temperature solution. In figure 13, since all points on curves 6A through 6B lie below the R&W data points, one can conclude that the M30A1 grain that contacts the steel residual in the location and configuration depicted in figures 4 and 12 will not undergo sustained combustion.

4. Discussion

Temperatures in the M30A1 were expected to come close to the ignition data in R&W (*2*) because experiments conducted here indicated that a V_s of 433 m/s resulted in threshold ignition of the propellant. The results reported here suggest that the methodology under-predicts the temperatures generated in the M30A1 by the hot steel residual.

Several uncertainties in our analysis may have contributed to the model's under-prediction of the propellant temperatures. The CTH model used density and dilation constants for the target plate that were representative of aluminum instead of titanium. This may have contributed to the under prediction of plastic deformation in the FSP calculated by CTH (8.5% increase in diameter vs. 12.5% for experimental, see figure 9). It is possible that with the proper titanium constants, CTH would have calculated more deformation and higher temperatures in the residual FSP. This would translate to higher temperatures calculated by LS-DYNA within the propellant. Our analysis also used a simplified geometry in LS-DYNA where the propellant grain was in contact with the heated region of the residual FSP, but not with the absolute hottest node in the FSP's heated leading edge. Additionally, the temperature computing algorithms in CTH have a limited predictive capability; therefore, we were unable to experimentally verify the temperature in the residual FSP.

Despite the uncertainties in our analysis, the methodology is promising and has sufficient flexibility to model other materials and provide ignition predictions, given accurate inputs and ignition temperature data.

5. Conclusions

The results of two sets of experiments are presented in this report. These experiments measured the ignition threshold V_s and V_r for two different steel RCC FSP masses, 830 gr and 208 gr, targeting two thicknesses of titanium plate armor, 0.25 in. and 0.5 in., respectively. We used these experiments to develop a computer simulation method for modeling and predicting the conductive thermal ignition of an energetic material by the residual steel penetrators. Our method employed two computer codes in series, CTH and LS-DYNA. The codes were coupled using a intermediate process to input the temperature field results produced by CTH into LS-DYNA for the heat conduction analysis. Using this method, we were able to model the entire event from the armor perforation to the propellant ignition.

The method was used to model the perforation of a 0.25 in. thick titanium plate by an 830 gr FSP with a V_s of 433 m/s and the subsequent contact of an M30A1 propellant grain with the hot steel residual. Heat conduction was neglected in the steel-titanium perforation analysis, performed with CTH. Deformation and motion were neglected in the post-processing heat conduction analysis performed with LS-DYNA. The temperature field, as a function of time within the M30A1 grain, was compared with data in R&W (*2*) for ignition time as a function of temperature. The temperature field in the M30A1 grain never reached the ignition temperature data in R&W (*2*), indicating a prediction of no ignition.

References

1. Gerri, N.J.; Berning, E. *Modeling Thermal Ignition of Energetic Materials*; ARL-TR-3369; U.S. Army Research Laboratory: Aberdeen Proving Ground, MD, 2004.

2. Rocchio, J.J.; Wires, R.A. *A Study of the Thermal Initiation, Cookoff, of M30 Propellants*; ARBRL-MR- 2847; Army Ballistic Research Laboratories: Aberdeen Proving Ground, MD, June 1978.

3. MIL-STD-2105C. Test Method Standard For Hazard Assessment Tests for Non-Nuclear Munitions. Prepared by the Naval Surface Warfare Center, Standardization Branch (Code 8420), Indian Head, MD, 20640-5035, July 14, 2003.

4. Raftenberg, M.N.; Meyer, H.W.; Clarke, J.A. *Coupling Between CTH and LS-DYNA for Thermal Postprocessing: Application to Propellant Cookoff From a Residual Penetrator*; ARL-TR-3924; U.S. Army Research Laboratory: Aberdeen Proving Ground, MD, 2006.

5. Raftenberg, M.N.; Meyer, H.W. Checking For Propellant Thermal Initiation From Contact With A Residual Penetrator; LS-DYNA Thermal Post-Processing of CTH Results, *Proceedings of JANNAF 2006*, San Diego, CA, pending publication.

6. Johnson, G.R.; Cook. W.H. Fracture Characteristics of Three Metals Subjected to Various Strains, Strain Rates, Temperatures and Pressures. *Engineering Fracture Mechanics* **1985**, 21, 31–48.

7. Miller, M.S. *Thermophysical Properties of Six Solid Gun Propellants*; ARL-TR-1322; U.S. Army Research Laboratory: Aberdeen Proving Ground, MD, 1997.

Abbreviations and Acronyms

3D	three-dimensional
ARL	U.S. Army Research Laboratory
cal	caliber
CSC	Courant Stability Criterion
CTH	an Eulerian shock-physics code
ELI	extra low interstitial
FSP	fragment simulating projectile
gr	grain
HE	high explosive
LS-DYNA	a Lagrangian hydrocode
R&W	Rocchio and Wires
RCC	right circular cylinder
SLAD	Survivability/Lethality Analysis Directorate
V_r	residual velocity
V_s	striking velocity

Distribution List

No. of Copies	Organization
1 elec	ADMNSTR DEFNS TECHL INFO CTR DTIC OCP 8725 JOHN J KINGMAN RD STE 0944 FT BELVOIR VA 22060-6218
6 CDs	US ARMY RSRCH LAB IMNE ALC IMS MAIL & RECORDS MGMT (1 CD) AMSRD ARL D J M MILLER (1CD) AMSRD ARL CI OK TL TECHL LIB (2 CDs) AMSRD ARL CI OK T TECHL PUB (2 CDs), 2800 POWDER MILL ROAD ADELPHI MD 20783-1197
1 CD	US ARMY RESEARCH LABORATORY ATTN AMSRD MAILROOM VAULT ATTN R REYNA BLDG 1624 WSMR NM 88002-5513
1CD	US ARMY RESEARCH LAB AMSRD CI OK TP TECHL LIB ATTN T LANDFRIED APG MD 21005
1 HC	US ARMY RSRCH DEV & ENGRG CMD SYSTEMS OF SYSTEMS INTEGRATION AMSRD SS T 6000 6TH ST STE 100 FORT BELVOIR VA 22060-5608
1 HC	USARL AMSRD ARL SL EW J NOWAK FORT MONMOUTH NJ 07703-5601
1 HC	US ARMY DEV TEST COM CSTE DTC TT T APG MD 21005-5055
1 HC	DIRECTOR US ARMY RESEARCH LAB IMNE ALC IMS 2800 POWDER MILL RD ADELPHI MD 20783-1197
1 HC	DIR USARL AMSRD ARL CI OK TP T LANDFRIED BLDG 4600 APG MD 21005-5055
1 HC	UNDER SECY OF THE ARMY DUSA TE H C DUBIN RM 5D564 CRYSTAL GATEWAY II 1225 S CLARK ST STE 1410 ARLINGTON VA 22202-4301
1 HC	DIRECTOR FORCE DEV DAMO FDZ RM 3A522 460 ARMY PENTAGON WASHINGTON DC 20310-0460
1 HC	US ARMY TRADOC ANL CTR ATRC W A KEINTZ WSMR NM 88002-5502
1 HC	USARL AMSRD ARL SL E R FLORES WSMR NM 88002-5513
1 HC	US ARMY EVALUATION CTR CSTE AEC SVE R LAUGHMAN 4120 SUSQUEHANNA AVE APG MD 21005-3013

No. of Copies	Organization
42 HCs	US ARMY RESEARCH LABORATORY
4 CDs	AMSRD ARL WM TD
1 elec	M RAFTENBERG (5 HCs, 1 CD)
	H MEYER (5 HCs, 1 CD)
	T BJERKE
	AMSRD ARL SL BE
	L ROACH
	E FIORAVANTE
	M MAHAFFEY
	J ABELL
	K BATES (5 HCs, 2 CDs, 1 elec)
	AMSRD ARL SL BM
	D FARENWALD
	M PERRY
	R SAUCIER
	A DIETRICH
	A PRAKASH
	A MIKHAIL
	T MALLORY
	G BRADLEY
	C BARKER
	D LYNCH
	G MANNIX
	AMSRD ARL SL BS
	W WINNER
	D HISLEY
	E.O. DAVISSON
	M GILLICH
	J AUTEN
	M KUNKEL
	AMSRD ARL SL BD
	R GROTE
	F MARSH
	P DOMINICK
	L MOSS
	AMSRD ARL HR MB
	P FEDELE
	APG MD 21005-5066

No. of Copies	Organization
14 HC	DIR USARL
	AMSRD ARL SL
	J BEILFUSS
	J FRANZ
	P TANENBAUM
	AMSRD ARL SL BM
	M PERRY
	AMSRD ARL SL BB
	S SNEAD
	AMSRD ARL SL BD
	R GROTE
	AMSRD ARL SL BE
	L ROACH
	AMSRD ARL SL BM
	D FARENWALD
	AMSRD ARL SL BS
	W WINNER (4 HCS)
	AMSRD ARL SL EC
	J FEENEY
1 HC	ASST SECY ARMY
	ACQSTN LOGISTICS & TECH
	SAAL ZP RM 2E661
	103 ARMY PENTAGON
	WASHINGTON DC 20310-0103
1 HC	ASST SECY ARMY
	ACQSTN LOGISTICS & TECH
	SAAL ZS RM 3E448
	103 ARMY PENTAGON
	WASHINGTON DC 20310-0103
TOTAL:	82 (2 Electronic, 12 CDs, and 68 HCs)